

World Journal of *Clinical Oncology*

World J Clin Oncol 2022 November 24; 13(11): 866-942



REVIEW

- 866 Influence of *Helicobacter pylori* oncoprotein CagA in gastric cancer: A critical-reflective analysis
Freire de Melo F, Marques HS, Rocha Pinheiro SL, Lemos FFB, Silva Luz M, Nayara Teixeira K, Souza CL, Oliveira MV

ORIGINAL ARTICLE**Basic Study**

- 880 Folate receptor-targeted near-infrared photodynamic therapy for folate receptor-overexpressing tumors
Aung W, Tsuji AB, Hanaoka K, Higashi T

Retrospective Cohort Study

- 896 Is it possible to adopt the same oncological approach in urgent surgery for colon cancer?
Yoshida BY, Araujo RLC, Farah JFM, Goldenberg A
- 907 Epidemiologic risk factors for patients admitted with chronic pancreatitis and pancreatic ductal adenocarcinoma in the United States
Lew D, Kamal F, Phan K, Randhawa K, Cornwell S, Bangolo AI, Weissman S, Pandol SJ
- 918 Efficacy of texture analysis of pre-operative magnetic resonance imaging in predicting microvascular invasion in hepatocellular carcinoma
Sim JZT, Hui TCH, Chuah TK, Low HM, Tan CH, Shelat VG

SYSTEMATIC REVIEWS

- 929 Gut microbiota diversity and composition in predicting immunotherapy response and immunotherapy-related colitis in melanoma patients: A systematic review
Oey O, Liu YY, Sunjaya AF, Simadibrata DM, Khattak MA, Gray E

ABOUT COVER

Editorial Board Member of *World Journal of Clinical Oncology*, Mamdouh M El-Shishtawy, Professor, Department of Biochemistry, Faculty of Pharmacy, Mansoura University, Mansoura, 35516, Dakahlia Governorate, Egypt.
mshisht@mans.edu.eg

AIMS AND SCOPE

The primary aim of *World Journal of Clinical Oncology (WJCO, World J Clin Oncol)* is to provide scholars and readers from various fields of oncology with a platform to publish high-quality basic and clinical research articles and communicate their research findings online.

WJCO mainly publishes articles reporting research results and findings obtained in the field of oncology and covering a wide range of topics including art of oncology, biology of neoplasia, breast cancer, cancer prevention and control, cancer-related complications, diagnosis in oncology, gastrointestinal cancer, genetic testing for cancer, gynecologic cancer, head and neck cancer, hematologic malignancy, lung cancer, melanoma, molecular oncology, neurooncology, palliative and supportive care, pediatric oncology, surgical oncology, translational oncology, and urologic oncology.

INDEXING/ABSTRACTING

The *WJCO* is now abstracted and indexed in PubMed, PubMed Central, Emerging Sources Citation Index (Web of Science), Reference Citation Analysis, China National Knowledge Infrastructure, China Science and Technology Journal Database, and Superstar Journals Database. The 2022 edition of Journal Citation Reports® cites the 2021 Journal Citation Indicator (JCI) for *WJCO* as 0.35.

RESPONSIBLE EDITORS FOR THIS ISSUE

Production Editor: Xiang-Di Zhang; Production Department Director: Xu Guo; Editorial Office Director: Yu-Jie Ma.

NAME OF JOURNAL

World Journal of Clinical Oncology

ISSN

ISSN 2218-4333 (online)

LAUNCH DATE

November 10, 2010

FREQUENCY

Monthly

EDITORS-IN-CHIEF

Hiten RH Patel, Stephen Safe, Jian-Hua Mao, Ken H Young

EDITORIAL BOARD MEMBERS

<https://www.wjgnet.com/2218-4333/editorialboard.htm>

PUBLICATION DATE

November 24, 2022

COPYRIGHT

© 2022 Baishideng Publishing Group Inc

INSTRUCTIONS TO AUTHORS

<https://www.wjgnet.com/bpg/gerinfo/204>

GUIDELINES FOR ETHICS DOCUMENTS

<https://www.wjgnet.com/bpg/GerInfo/287>

GUIDELINES FOR NON-NATIVE SPEAKERS OF ENGLISH

<https://www.wjgnet.com/bpg/gerinfo/240>

PUBLICATION ETHICS

<https://www.wjgnet.com/bpg/GerInfo/288>

PUBLICATION MISCONDUCT

<https://www.wjgnet.com/bpg/gerinfo/208>

ARTICLE PROCESSING CHARGE

<https://www.wjgnet.com/bpg/gerinfo/242>

STEPS FOR SUBMITTING MANUSCRIPTS

<https://www.wjgnet.com/bpg/GerInfo/239>

ONLINE SUBMISSION

<https://www.f6publishing.com>

Basic Study

Folate receptor-targeted near-infrared photodynamic therapy for folate receptor-overexpressing tumors

Winn Aung, Atsushi B Tsuji, Kenjiro Hanaoka, Tatsuya Higashi

Specialty type: Oncology**Provenance and peer review:**

Unsolicited article; Externally peer reviewed.

Peer-review model: Single blind**Peer-review report's scientific quality classification**

Grade A (Excellent): 0

Grade B (Very good): B, B

Grade C (Good): 0

Grade D (Fair): 0

Grade E (Poor): 0

P-Reviewer: Jabbarpour Z, Iran;
Janmohammadi P, Iran**Received:** August 3, 2022**Peer-review started:** August 3, 2022**First decision:** August 29, 2022**Revised:** September 12, 2022**Accepted:** October 18, 2022**Article in press:** October 18, 2022**Published online:** November 24,
2022**Winn Aung, Atsushi B Tsuji, Tatsuya Higashi**, Department of Molecular Imaging and Theranostics, Institute for Quantum Medical Science, National Institutes for Quantum and Radiological Science and Technology, Chiba 263-8555, Japan**Kenjiro Hanaoka**, Faculty of Pharmacy and Graduate School of Pharmaceutical Sciences, Keio University, Tokyo 105-8512, Japan**Corresponding author:** Winn Aung, MBBS, PhD, Senior Researcher, Department of Molecular Imaging and Theranostics, Institute for Quantum Medical Science, National Institutes for Quantum and Radiological Science and Technology, 4-9-1 Anagawa, Inage-ku, Chiba 263-8555, Japan. winn.aung@qst.go.jp**Abstract****BACKGROUND**

Photodynamic therapy (PDT) is a minimally invasive form of cancer therapy, and the development of a novel photosensitizer (PS) with optimal properties is important for enhancing PDT efficacy. Folate receptor (FR) membrane protein is frequently overexpressed in 40% of human cancer and a good candidate for tumor-specific targeting. Specific active targeting of PS to FR can be achieved by conjugation with the folate moiety. A folate-linked, near-infrared (NIR)-sensitive probe, folate-Si-rhodamine-1 (FolateSiR-1), was previously developed and is expected to be applicable to NIR-PDT.

AIM

To investigate the therapeutic efficacy of NIR-PDT induced by FolateSiR-1, a FR-targeted PS, in preclinical cancer models.

METHODS

FolateSiR-1 was developed by conjugating a folate moiety to the Si-rhodamine derivative through a negatively charged tripeptide linker. FR expression in the designated cell lines was examined by western blotting (WB). The selective binding of FolateSiR-1 to FR was confirmed in FR overexpressing KB cells (FR+) and tumors by fluorescence microscopy and *in vivo* fluorescence imaging. Low FR expressing OVCAR-3 and A4 cell lines were used as negative controls (FR-). The NIR light (635 ± 3 nm)-induced phototoxic effect of FolateSiR-1 was evaluated by cell viability imaging assays. The time-dependent distribution of FolateSiR-1 and its specific accumulation in KB tumors was determined using *in vivo* longitudinal fluorescence imaging. The PDT effect of FolateSiR-1 was evaluated in KB tumor-

bearing mice divided into four experimental groups: (1) FolateSiR-1 (100 µmol/L) alone; (2) FolateSiR-1 (100 µmol/L) followed by NIR irradiation (50 J/cm²); (3) NIR irradiation (50 J/cm²) alone; and (4) no treatment. Tumor volume measurement and immunohistochemical (IHC) and histological examinations of the tumors were performed to analyze the effect of PDT.

RESULTS

High FR expression was observed in the KB cells by WB, but not in the OVCAR-3 and A4 cells. Substantial FR-specific binding of FolateSiR-1 was observed by *in vitro* and *in vivo* fluorescence imaging. Cell viability imaging assays showed that NIR-PDT induced cell death in KB cells. *In vivo* longitudinal fluorescence imaging showed rapid peak accumulation of FolateSiR-1 in the KB tumors 2 h after injection. *In vivo* PDT conducted at this time point caused tumor growth delay. The relative tumor volumes in the PDT group were significantly reduced compared to those in the other groups [5.81 ± 1.74 (NIR-PDT) *vs* 12.24 ± 2.48 (Folate-SiR-1), *vs* 11.84 ± 3.67 (IR), *vs* 12.98 ± 2.78 (Untreated), at Day 16, *P* < 0.05]. IHC analysis revealed reduced proliferation marker Ki-67-positive cells in the PDT treated tumors, and hematoxylin-eosin staining revealed features of necrotic- and apoptotic cell death.

CONCLUSION

FolateSiR-1 has potential for use in PDT, and FR-targeted NIR-PDT may open a new effective strategy for the treatment of FR-overexpressing tumors.

Key Words: Photodynamic therapy; Near-infrared; Photosensitizer; Folate receptor; Fluorescence; Cancer

©The Author(s) 2022. Published by Baishideng Publishing Group Inc. All rights reserved.

Core Tip: Photodynamic therapy (PDT) is a minimally invasive cancer therapy and photosensitizers (PS) with optimal properties are crucial for enhancing the efficacy of PDT. We evaluated the therapeutic efficacy of a folate receptor (FR)-targeted, near-infrared (NIR)-sensitive PS (FolateSiR-1). FolateSiR-1 showed FR specificity *in vitro* and *in vivo* and functions as a tumor-damaging PS by inducing necrosis, apoptosis, and cell growth inhibition upon activation with NIR light. Our findings suggest that FolateSiR-1 is effective in FR-targeted NIR-PDT with low side effects and has potential for presenting new and effective treatment options for FR-overexpressing tumors.

Citation: Aung W, Tsuji AB, Hanaoka K, Higashi T. Folate receptor-targeted near-infrared photodynamic therapy for folate receptor-overexpressing tumors. *World J Clin Oncol* 2022; 13(11): 880-895

URL: <https://www.wjgnet.com/2218-4333/full/v13/i11/880.htm>

DOI: <https://dx.doi.org/10.5306/wjco.v13.i11.880>

INTRODUCTION

Cancer incidence and mortality is continually growing worldwide. GLOBOCAN 2020 estimated that there were 19.3 million new cancer cases and almost 10 million cancer deaths in 2020 and the global cancer burden is expected to reach 28.4 million cases in 2040[1]. Molecular-targeted approaches with various therapeutic modalities are expected to provide effective cancer diagnosis and treatment.

Photodynamic therapy (PDT) is one of the emerging options to combat various cancer types along with other conventional therapies such as surgery, chemotherapy, radiation therapy, and immunotherapy[2]. It is approved for the clinical treatment of several tumor types and certain non-malignant diseases as a minimally invasive therapy[3]. Although the precise mechanisms of tumor cell death by photodamage are not yet fully understood, they involve necrosis, apoptosis, tumor blood vessel damage, and nonspecific activation of the immune response against tumor cells[4]. Cell death through PDT generally occurs through a combination of these mechanisms, and no single pathway leads to cell death[5]. Photodynamic therapy involves the administration of a light-sensitive photosensitizer (PS) followed by the irradiation of targeted tumors with light corresponding to the specific absorbance wavelength of the PS[3]. Light activated PS accumulated in the cancer tissue leads to the local generation of reactive oxygen species (ROS), such as highly reactive singlet oxygen and/or radicals, which kill tumor cells through necrosis and cause tumor regression[6,7]. However, off-target toxicities and PS metabolic problems were encountered in clinical trials, and therefore, only a few PSs have been approved for anti-cancer therapies[8]. The tumor selectivity of the PS improves tumor localization in PDT, enhances tumor destruction, and reduces the side effects due to off-target localization[9].

Moreover, effective targeting reduces the required PS dose which additionally limits side effects. Tumor-localizing properties are generally dependent on the passive enhanced permeability and retention effect[10]. More effective active targeting is expected and achieved by diverse approaches such as the conjugation of receptor ligands, antibodies, carrier proteins, carbohydrates, and loading into targeted nanoparticles[11-14].

The first-generation of PSs were hematoporphyrin derivatives, and the first PS to be clinically used for cancer therapy was porfimer sodium (Photofrin®)[4]. Its poor tissue selectivity, low light absorption, and weak tissue penetration of emission demanded the development of second-generation PSs, porphyrinoids, and non-porphyrin compounds[15]. Moreover, third-generation PSs were developed by conjugating carrier biomolecules, such as receptor ligands or antibodies, to the second-generation PSs to selectively target tumors[4]. Nevertheless, the number of new clinically approved PSs remains low, and researchers are developing new improved PSs.

Folate receptor (FR) membrane protein is frequently overexpressed in 40% of human cancer types, including ovary, breast, head and neck, endometrium, lung, bladder, pancreatic, colon, and kidney cancer, whereas its expression is restricted to normal tissues[16]. It binds to extracellular folate with very high affinity and can physically deliver folate into the cell through endocytosis[17]. Therefore, FR is a good candidate for tumor-specific PS targeting[9,18]. Specific active targeting of PS to FR present on the cancer cell surface can be achieved by conjugation with the folate moiety[19]. Several studies have shown that some PSs conjugated with folic acid *via* appropriate linkers increase tumor uptake and enhance the efficacy of PDT. For instance, conjugation of folic acid to *meta*-tetra(hydroxyphenyl)chlorin (*m*-THPC)-like PS[20] and chlorin-based PS pheophorbide-a[21] has been reported. In addition, various materials such as polymers, nanomaterials, polysaccharides and cyclodextrins have been explored to overcome the shortcoming of PSs *via* tissue-specific delivery[22]. For example, folate-conjugated micelles containing temoporfin[23] and polydopamine nanoparticles conjugated with folic acid[24] showed potential for therapeutic applications. Kim *et al*[22] showed that ROS-sensitive and FR-targeted nanophotosensitizer conjugates are promising candidates for PDT of cervical cancer. Kato *et al*[25,26] reported that folate-porphyrin-lipid nanoparticles induced the selective destruction of lung cancer and malignant pleural mesothelioma in a preclinical model based on FR targeting. Baydoun *et al*[27] proved the efficacy of a new PS (pyropheophorbide a-polyethylene glycol-folic acid) on human ovarian cancer cells. Quilbe *et al*[28] developed a new PS targeting FR, protected by patent (WO2019 016397-A1) and evaluated its PDT efficacy on a mouse model of pancreatic cancer. These latest state-of-the-art studies encourage the use of folate-mediated PSs in tumor-targeted photodynamic therapy. In an alternative approach called photoimmunotherapy (PIT), PSs conjugated with monoclonal antibodies that have high affinity to tumor specific antigens instead of using receptor ligands have also investigated[29,30].

PS targeting was developed or improved by conjugating fluorophores to tumor-seeking molecules [31]. We previously developed a folate-linked near-infrared (NIR)-sensitive probe, folate-Si-rhodamine-1 (FolateSiR-1, $Abs_{max}/Em_{max} = 652/674$ nm, and fluorescence quantum yield of 7.6%) using folate glutamate as a tumor-seeking agent, a negatively charged peptide linker, and rhodamine derivative, 2,5-diCOOH SiR650, as a photoactive component (Figure 1A)[32]. Folate receptor α contains a folate-binding pocket[33]. The folate pteroate moiety is buried inside the receptor, whereas its glutamate moiety is solvent-exposed and protrudes from the pocket, which allows its conjugation to the fluorophore without adversely affecting FR α binding[33]. We chose to conjugate the linker to the folate glutamate moiety, as this allowed high affinity- and highly selective binding of FolateSiR-1 probe to FR [34]. One of the main drawbacks of currently approved PDTs is the insufficient penetration of light during treatment. This may be overcome by using NIR absorbing PSs[32] and appropriate NIR light sources because red and infrared light penetrate tissue more deeply than other visible light[3]. The photophysical properties of FolateSiR-1 and the wavelength of our laser system (635 ± 3 nm) used in this study resolved this issue. Fluorophores emitting NIR light in the phototherapeutic window (650-900 nm) are most suitable due to high tissue penetration and low autofluorescence, which results in a low background signal[35]. FolateSiR-1 exhibited very low background fluorescence and showed a high ratio of tumor-to-background fluorescent intensity[32].

In this study, we evaluated the *in vitro* and *in vivo* tumor specific targeting- and photodynamic activity of FolateSiR-1 using high-FR-expressing-KB cells (FR+) and low-FR-expressing-OVCAR-3 cells (Low FR). We revealed the potential of FolateSiR-1 as a candidate for use in the PDT of cancer by assessing its phototoxic cell death and antitumor effects. In addition, the cell death mode induced by FolateSiR-1-based PDT was investigated.

MATERIALS AND METHODS

Cell lines and culture

The human oral epidermoid carcinoma cell line, KB (a HeLa subline), and human epithelial ovarian cancer cell line, OVCAR-3, were purchased from the American Type Culture Collection (ATCC) (Manassas, VA, United States). The KB cells were cultured in Eagles's minimum essential medium (EMEM) (Wako Pure Chemical Corp., Osaka, Japan) supplemented with 10% fetal bovine serum (FBS)

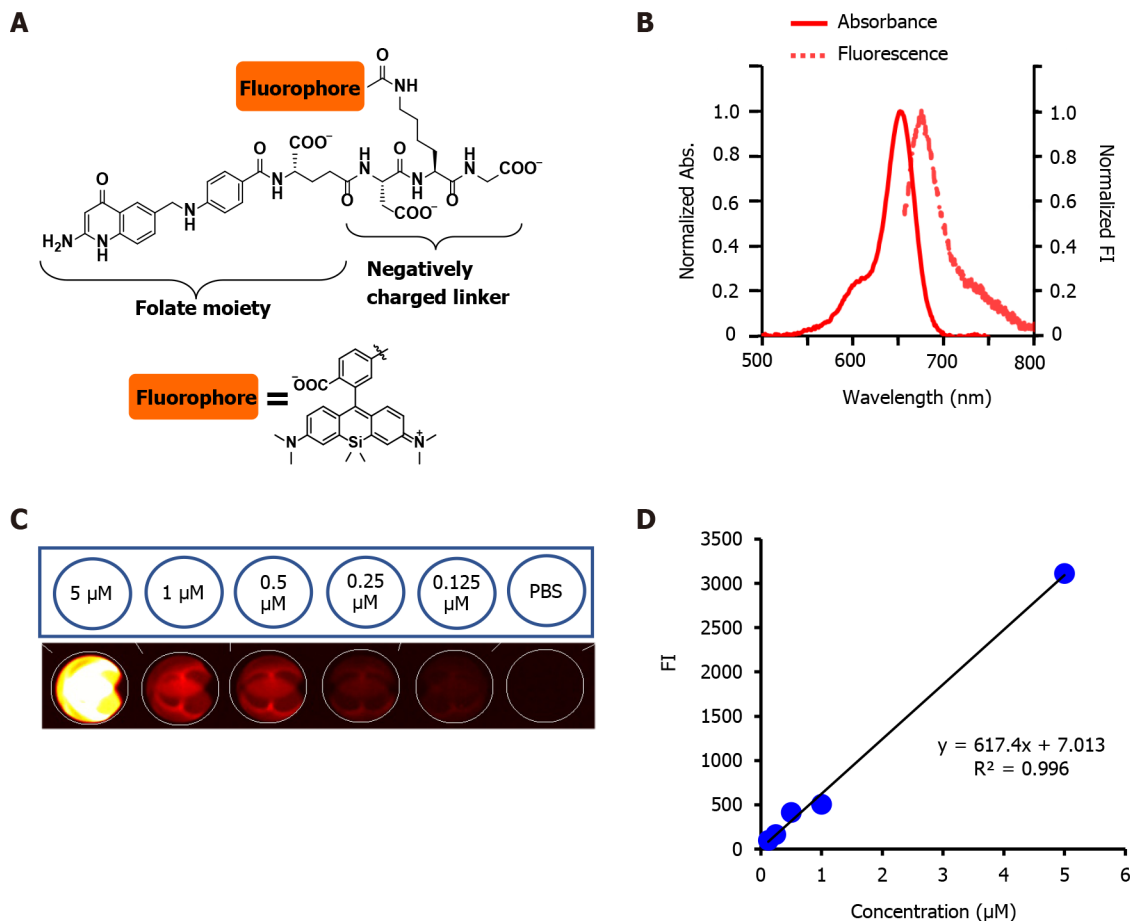


Figure 1 Folate-Si-rhodamine-1 characteristics. A: Molecular design and chemical structure of folate-Si-rhodamine-1 (FolateSiR-1); B: Absorption and emission spectra of 1 $\mu\text{mol/L}$ FolateSiR-1 in 100 mmol/L sodium phosphate buffer (pH 7.4) containing 0.1% DMSO: maximum absorption = 652 nm; maximum emission = 674 nm; C: Fluorescence images of FolateSiR-1 at a concentration of 5, 1, 0.5, 0.25, and 0.125 $\mu\text{mol/L}$ in a 96-well plate captured using the VISQUE fluorescence imaging system; D: FolateSiR-1 concentration vs fluorescence signal intensity. Abs: Absorbance; FI: Fluorescence signal intensity; μM : $\mu\text{mol/L}$.

(Gibco, Life Technologies Japan Ltd., Tokyo, Japan), 100 U/mL penicillin-G sodium, and 100 $\mu\text{g/mL}$ streptomycin sulfate (Wako) at 37 °C in a humidified incubator containing 5% CO_2 . The A4 cell line is an immortalized mouse fibroblast cell line established from mouse 3T3 cells and transfected with human epidermal growth factor receptor 2-expression vector. The OVCAR-3 cells and A4 cells were similarly cultured in RPMI 1640 medium (Wako) supplemented with 10% FBS (Gibco), 100 U/mL penicillin-G sodium, and 100 $\mu\text{g/mL}$ streptomycin sulfate (Wako).

FolateSiR-1 synthesis

FolateSiR-1 was designed and synthesized using folate glutamate as a tumor-seeking agent, a negatively charged peptide linker, and a rhodamine derivative, 2,5-diCOOH SiR650, as a photoactive component according to a previously described method[32]. Fluorescence spectroscopic analyses of FolateSiR-1 was conducted with a Hitachi F7000 spectrophotometer (Tokyo, Japan) using 2.5 nm excitation and emission slit widths and 700 V photomultiplier voltage. Different FolateSiR-1 concentrations (5, 1, 0.5, 0.25, 0.125 $\mu\text{mol/L}$) were prepared in 100 μL in a Nunc™ flat-bottom microplate (96 well, Black) (Thermo Fisher Scientific, Roskilde, Denmark). The fluorescence signal intensity (FI) was determined using a VISQUE InVivo Smart fluorescence imaging and analysis system (Vieworks Co., Ltd, Gyeonggi, Korea) equipped with HyperRed light filter set (Ex/Em = 630-680/690-740 nm).

Animal and tumor model

Ethics Committee-approved animal studies were conducted in accordance with the institutional guidelines of the Animal Care and Use of Committee of National Institutes for Quantum and Radiological Science and Technology. The animal protocol was designed to minimize pain or discomfort to the animals. Four-week-old male BALB/cAJcl-nu/nu mice were obtained from CLEA (Shizuoka, Japan), kept in an air-conditioned facility (23 °C) with an artificial 12 h light-dark cycle, 50% humidity, and provided autofluorescence-free food and water *ad libitum* for one week prior to experimentation. Development of tumor models involved subcutaneous inoculation of early passage cells (5×10^6 KB cells/site, 1×10^7 OVCAR-3 cells/site, or 5×10^6 A4 cells/site, all in 100 μL medium) into both femoral

regions of nude mice. Mice were anesthetized with isoflurane during the experimental procedure. All animals were euthanized by cervical dislocation under anesthesia (inhalation of isoflurane) for tumor tissue collection.

Western blot analysis

Folate receptor expression in designated cells was examined by western blotting (WB). First, whole-cell lysate was prepared using radioimmunoprecipitation assay buffer (Wako) containing protease inhibitor cocktail (P8340; Sigma-Aldrich, St. Louis, MO, United States). Total protein concentration was determined using a NanoDrop One spectrophotometer (Thermo Fisher Scientific, Wilmington, DE, United States). Next, 50 µg of cell lysate protein samples were separated using 4%-20% polyacrylamide gel (ATTO Corporation, Tokyo, Japan) and transferred onto an Immobilon-P membrane (Millipore, Billerica, MA, United States). Mouse monoclonal antibody anti-FR of human origin (E-11) (Santa Cruz Biotechnology, Santa Cruz, CA, United States) (1:200 dilution) and goat polyclonal anti-human actin antibody (Santa Cruz Biotechnology) (1:500 dilution) were used as primary antibodies. Horseradish peroxidase (HRP)-linked anti-mouse IgG antibody (GE Healthcare, Little Chalfont, United Kingdom) (1:1000 dilution) and HRP-linked anti-goat IgG antibody (Santa Cruz Biotechnology) (1:1000 dilution) were used as secondary antibodies. The Enhanced Chemiluminescence Plus detection system (GE Healthcare) was used to visualize the immunoreactive bands.

Fluorescence microscopy

KB cells (1×10^5 cells/well) were seeded onto an EZVIEW glass bottom culture plate (24 well, black; IWAKI, Shizuoka, Japan) in complete EMEM medium (1 mL) and incubated for 24 h at 37 °C. The media was removed and each well was washed with PBS, subsequently, fresh medium was added with or without FolateSiR-1 (2.5 µmol/L in 0.5% DMSO) and incubated overnight at 37 °C. The medium was discarded, cells were washed with phenol red free EMEM α medium (Wako) two times, and each well was refilled with the same medium. The OVCAR-3 cells (5×10^5 cells/well) and A4 cells (1×10^5 cells/well) were prepared using RPMI 1640, and the cells were observed using a Keyence BZ-X700 fluorescence microscope (Keyence Japan Co, Ltd, Osaka, Japan) with an Ex/Em 590-650/665-732 nm filter for FolateSiR-1. The same exposure time was consistently used. Phase-contrast images were also captured.

Cell viability imaging

KB cells (1.5×10^5 cells/well) were seeded onto a EZVIEW glass bottom culture plate (24 well, black; IWAKI) in complete EMEM medium overnight at 37 °C. Spent medium was replaced with fresh medium with or without FolateSiR-1 (2.5 µmol/L in 0.5% DMSO) and the KB cells were incubated overnight. Next, the medium was discarded, cells were washed with phenol red free medium (Wako), and subsequently irradiated with NIR light from an infrared diode laser system (Laser Create Co., Tokyo, Japan) at 635 ± 3 nm and a power density of 10 J/cm² (0.1 W/cm² for 100 s). The distance between the sample and light source was set to 3 cm, and the light power was adjusted to 0.1 W/cm². The irradiation dose was measured using a Starlite thermal laser power sensor and optical power meter (OPHIR Japan, Saitama, Japan). After irradiation, each well was refilled with the same medium and incubated at 37 °C. Two hours later, two color staining assays were conducted using the ReadyProbes™ cell viability imaging kit (Thermo Fisher Scientific K.K, Tokyo, Japan) according to manufacturer's instructions. Nuclei of the viable cells and dead cells were stained with NucBlue® Live reagent and NucGreen® Dead reagent, respectively. Cell images were acquired with a Keyence BZ-X700 microscope (Keyence Japan Co, Ltd) with filter sets for NucBlue® (Ex/Em = 360/460 nm), NucGreen® (Ex/Em = 475/509 nm), and FolateSiR-1 (red, Ex/Em = 590-650/665-732 nm). Image acquisitions were conducted using similar exposure times.

Mice NIR fluorescence imaging

Intravenous injection of FolateSiR-1 (100 µmol/L in 100 µL saline and 10% DMSO) into the tail vein of tumor-bearing mice was followed by anesthetization and acquisition of fluorescent and white light images at the dorsal position. Pre-injection- and post-injection time points (5 min, 10 min, 15 min, 20 min, 30 min, 45 min, and 1 h, 2 h, 3 h, 4 h, 4.5 h, 5 h, 6 h, 24 h, and 48 h) were designated for longitudinal imaging. *In vivo* NIR fluorescence imaging was conducted using the VISQUE imaging system (Vieworks Co., Ltd.) equipped with HyperRed light filter (Ex/Em = 630-680/690-740 nm) using constant imaging parameters (exposure time: 100 ms, binning: 1×1 , light intensity: high, mode: low gain). Tumor FI was acquired by subtracting nearby background FI using CleVue software (Vieworks). Two mice with OVCAR-3 and KB tumors in their left and right femoral regions, respectively, were imaged to confirm FR-specific binding. Similarly to the other control samples, KB tumor-bearing mice that did or did not receive the FolateSiR-1 injection were imaged together, and the A4 (low FR) tumor-bearing mouse was imaged after PS injection.

In vivo tumor PDT

Subcutaneous tumor lengths peaked at approximately 6-10 mm nine days after xenografting. These

mice were randomly assigned to one of the four groups ($n = 5$ in each group), and treatment was conducted using the designated schedule. FolateSiR-1 (100 $\mu\text{mol/L}$) was initially administered intravenously. After 2 h, the tumor was exposed to NIR light from a Diode Laser system (Laser Create Co.) at 635 ± 3 nm and 50 J/cm^2 (0.25 W/cm^2 for 200 s). The distance between the tumor and NIR light source was set to 3 cm. Whole body of the mouse, except for the tumor area, was shielded from the light using aluminum foil. Group 1 received PS injection, group 2 received PS injection followed by light irradiation at 2 h post-injection, group 3 was only irradiated, and group 4 received no treatment. Tumor sizes of all mice ($n = 8$ for each) were measured twice a week over 16 d using calipers, and volumes were calculated according to the formula: $\text{volume (mm}^3) = [\text{length (mm)}] \times [\text{width (mm)}]^2 \times 0.5$. The relative tumor volume was calculated based on the ratio of the volume on the indicated day and the starting volume prior to the treatment. Mice were weighed twice a week, while the skin condition of the light exposed area, and general conditions of the mice were monitored daily.

Immunohistochemical- and histological analysis

Twenty-four h after irradiation, a mouse from each group was sacrificed. The tumors were excised, fixed in 4% paraformaldehyde, embedded in paraffin, and cut into 5 μm -slices. Serial tissue sections were rehydrated and subjected to antigen retrieval for immunohistochemical (IHC) analysis. The sections were then stained for Ki-67 cell proliferation marker[36] using anti-human Ki-67 polyclonal antibody (Dako Denmark, Glostrup, Denmark) (1:200 dilution) as previously described[37]. Mouse monoclonal anti-FR antibody of human origin (E-11) (Santa Cruz Biotechnology) (1:200 dilution) was used to investigate tumor FR expression. Serial sections were stained with hematoxylin and eosin (H&E) dye to examine histopathological changes. Slides were examined with an Olympus BX43 microscope (Tokyo, Japan).

Statistical analysis

The quantitative results are presented as the mean \pm SD. Relative tumor volume differences between groups were determined using ANOVA (two-factor with replication; Excel, Microsoft, Redmond, WA, United States), followed by Tukey's test. P values < 0.05 were considered statistically significant.

RESULTS

FolateSiR-1 conjugate characteristics

FolateSiR-1 probe (molecular weight 1232.78, **Figure 1A**) was developed from a Si-rhodamine derivative containing a carboxy group at the benzene moiety coupled to a folate ligand moiety through a negatively charged tripeptide[32]. FolateSiR-1 is expected to possess high affinity to FR with a tumor-seeking character of folate glutamate[38]. Rhodamine derivative 2,5-diCOOH SiR650 serves as a photoactive component. Maximum absorption and emission wavelengths of 1 $\mu\text{mol/L}$ FolateSiR-1 in 100 mmol/L sodium phosphate buffer at pH 7.4 were 652 nm and 674 nm, respectively (**Figure 1B**)[32]. FolateSiR-1 fluorescence emission was most clearly visualized with HyperRed light filter (Ex/Em = 630-680/690-740 nm) using the VISQUE imaging system (**Figure 1C**). The quantitative evaluation of FI revealed that the linear correlation coefficient between fluorescence and FolateSiR-1 concentration was 0.996 (**Figure 1D**).

Folate receptor expression and FolateSiR-1 accumulation in cultured cells

High FR expression was observed in the KB cells by WB, but not in the OVCAR-3 and A4 cells (**Figure 2A**). Likewise, FolateSiR-1 accumulated in the KB cells at the cell membrane and their intracellular localization indicated substantial specific binding of FolateSiR-1 to FR and its internalization using fluorescence microscopy. However, this was not seen in almost any of the OVCAR-3 and A4 cells (**Figure 2B**). All three cell lines incubated in medium without FolateSiR-1 showed no fluorescence activity (data not shown).

Folate receptor-specific binding of FolateSiR-1 in in vivo tumors

Using the VISQUE imaging system 2 h after injecting FolateSiR-1 into tumor-bearing mice, the KB tumors inoculated in the right femoral regions showed high FI, while the OVCAR-3 tumors inoculated in the left femoral regions showed no FI (**Figure 2C**). Next, the KB tumor of the mouse that was administered FolateSiR-1 exhibited FI, but the negative control tumor of the mouse with no FolateSiR-1 injection did not (**Figure 2D**). Moreover, a mouse bearing A4 (low FR) tumor showed no FI (**Figure 2E**). After imaging, IHC examination of tumor tissue sections showed high FR expression in the KB tumor (**Figure 2F**). These results suggest that there was specific binding of FolateSiR-1 to FR in the tumors.

Phototoxic cell death induced by FolateSiR-1 mediated PDT

Immediate cell death induced by NIR-PDT was detected based on green colored cells by fluorescence microscopy, resulting from the staining with the NucGreen® Dead reagent, whereas viable cell nuclei

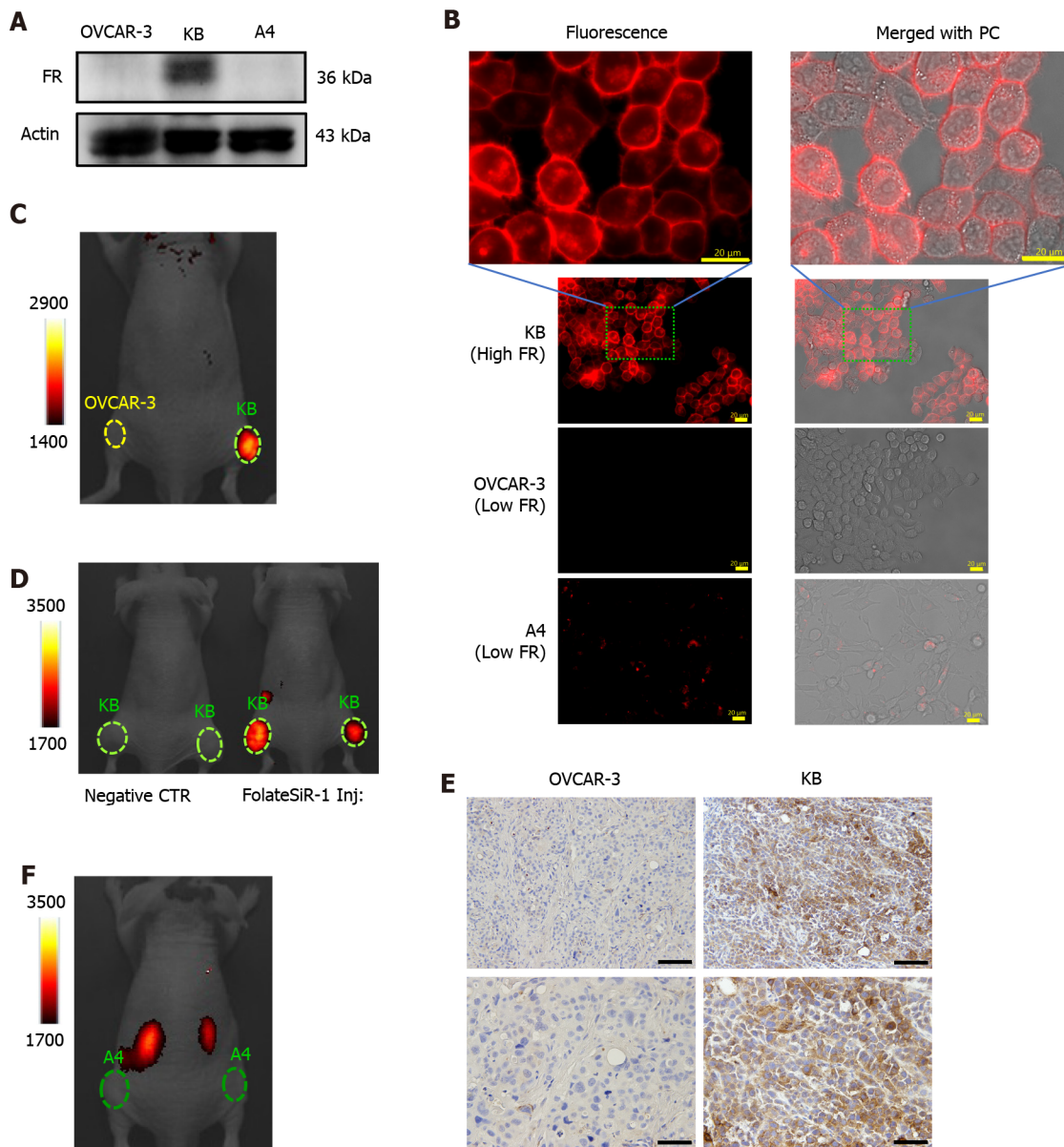


Figure 2 Folate receptor expression in designated cell lines and folate receptor-specific binding of folate-Si-rhodamine-1 in tumor *in vivo*.
 A: Folate receptor (FR) expression in cell lines OVCAR-3, KB, and A4 examined by western blotting; B: Cell lines were incubated with or without folate-Si-rhodamine-1 (FolateSiR-1) for 24 h and examined under a fluorescent microscope. FolateSiR-1 fluorescence was detected using the appropriate filters (Ex/Em 590-650/665-732 nm). The uppermost images are magnifications of the indicated portion of the lower image showing KB cells (scale bar = 20 μ m, 40 \times magnification, and 120 \times magnification for the upper most image); C: Near-infrared (NIR) fluorescence image of a representative mouse bearing subcutaneous KB (right) and OVCAR-3 (left) tumors at 2 h after receiving the FolateSiR-1 injection: KB tumor (FR+) showed high fluorescence signal intensity (FI), and OVCAR-3 tumor (low FR) did not; D: NIR fluorescence image of mice bearing KB tumors: the right mouse received the FolateSiR-1 injection showed FI, while the left mouse did not (negative control tumor) show no FI; E: NIR fluorescence image of a mouse bearing A4 (low FR) tumor showed no FI; F: Immunohistochemical analysis of tumor tissue sections for FR expression: KB tumor (right column), OVCAR-3 tumor (left column). Scale bar = 100 μ m, 20 \times magnification for upper panel, and scale bar = 50 μ m, 40 \times magnification, for lower panel. FR: Folate receptor; Ex: Excitation; Em: Emission; FI: Fluorescence signal intensity; FolateSiR-1: Folate-Si-rhodamine-1; PC: Phase-contrast; NIR: Near-infrared; CTR: Control.

were stained blue with NucBlue® Live reagent (Figure 3). No noticeable phototoxic cell death was observed with FolateSiR-1 treatment alone, light treatment alone, or no treatment (Figure 3).

In vivo FolateSiR-1 biodistribution in tumorbearing mice

Time-dependent distribution of FolateSiR-1 and its specific accumulation in the tumors was determined based on serial images of a representative mouse following FolateSiR-1 injection (Figure 4A). The quantified FI in the tumor rapidly increased, peaking approximately 2 h after injection, and almost disappearing over 24 h (Figure 4B). Moreover, in another experiment, decreased tumor FI was observed in the right tumor that received PDT after 30 min compared with that of the non-irradiated left tumor (Figure 5A). Although there was a time-dependent decrease of FI due to normal washout of the PS from the tumor, the degree of FI reduction in the tumor treated with PDT was greater than in the untreated

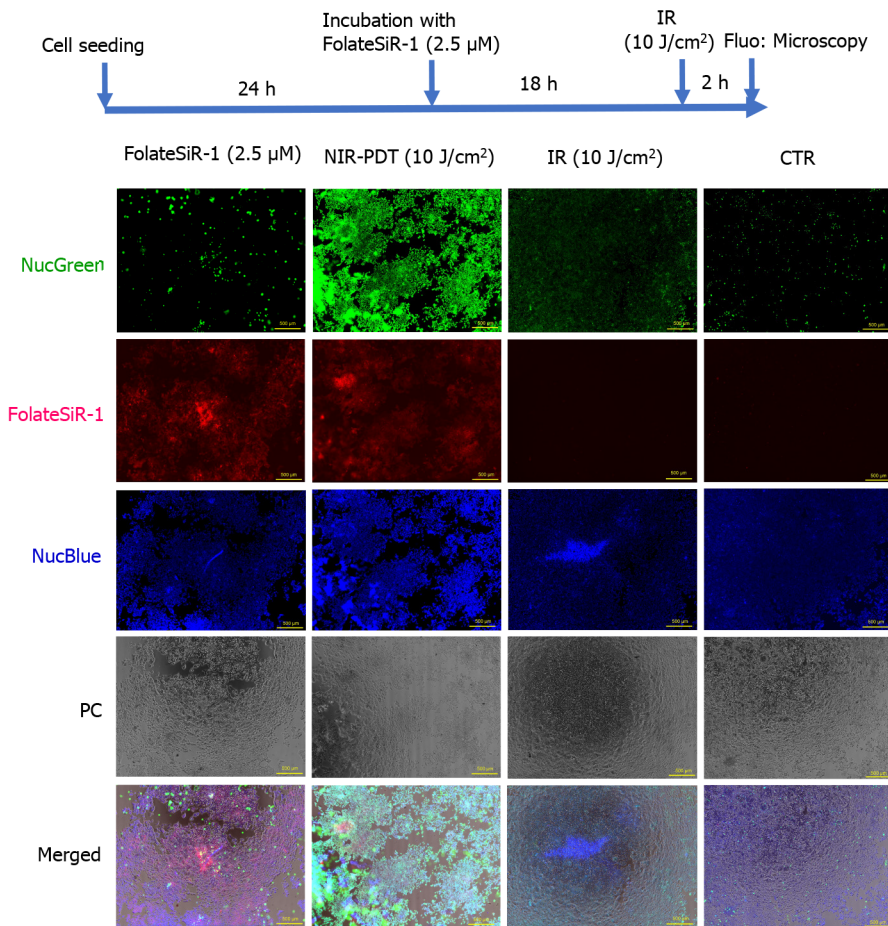


Figure 3 *In vitro* phototoxicity of folate-Si-rhodamine-1 after laser irradiation. The cells were stained using the reagents from the Cell viability imaging kit at 2 h after near-infrared photodynamic therapy (NIR-PDT). The nuclei of dead cells were stained with NucGreen® Dead reagent (green), while the viable cell nuclei were stained with NucBlue® Live reagent (blue). Rapid cell death-induced by PDT (10 J/cm²) and abundant dead cells were clearly noted. (scale bar = 500 μm, 10 × magnification). NIR-PDT: Near-infrared photodynamic therapy; IR: Laser irradiation; CTR: Control; NucGreen: NucGreen® Dead reagent; NucBlue: NucBlue® Live reagent; PC: Phase-contrast; μM: μmol/L.

tumor. Therefore, the percentage decrease of tumor FI was higher in the PDT-induced tumors (Figure 5B). Mice were euthanized shortly after *in vivo* imaging, with tumors and other organs removed and analyzed by the VISQUE imaging system. *Ex vivo* NIR images showed higher FI in tumor tissues compared with major organs, and higher FI in the right tumor compared with that of the left tumor. Meanwhile, FI from organs including the liver and kidney was barely visible (Figure 5C). *Ex vivo* results showed similar trends in data as that in *in vivo* imaging data.

***In vivo* PDT efficacy of FolateSiR-1 on tumor size**

The tumor-bearing mice were treated according to the scheme shown in Figure 6. Statistically significant tumor growth inhibition was observed after NIR-PDT treatment *vs* FolateSiR-1 treatment alone, NIR irradiation alone, and no treatment ($P < 0.05$, Figure 7A). No significant differences were observed amongst other groups. There was no significant body weight loss, skin damage, or abnormal general conditions in these mice (Figure 7B). Relatively decreased sizes of PDT-treated tumors were observed *ex vivo* 16 d after treatment compared with that in the other groups (Figure 7C).

Evaluation of tumor tissue response to PDT by IHC and histopathology

Proliferative factor Ki67 nuclear staining in the control tumor cells was observed by IHC analysis. In contrast, the tumor tissues treated with PDT showed weak staining and markedly reduced numbers of Ki-67-positive cells, suggesting that PDT inhibited tumor growth (Figure 8). Furthermore, PDT treated tumors showed rapid extensive damage with necrotic- and apoptotic cell death at the irradiated tumor site as indicated by H&E staining. PDT treated tumor cells showed some features of necrosis and apoptosis such as nuclear fading due to DNA degradation (karyolysis), anuclear necrotic cells with a glossier homogenous appearance, nuclear chromatin condensation (pyknosis), and nuclear fragmentation (karyorrhexis). No conspicuous damage was found in the tumors of the other control groups receiving FolateSiR-1 alone, irradiation alone, or no treatment (Figure 9).

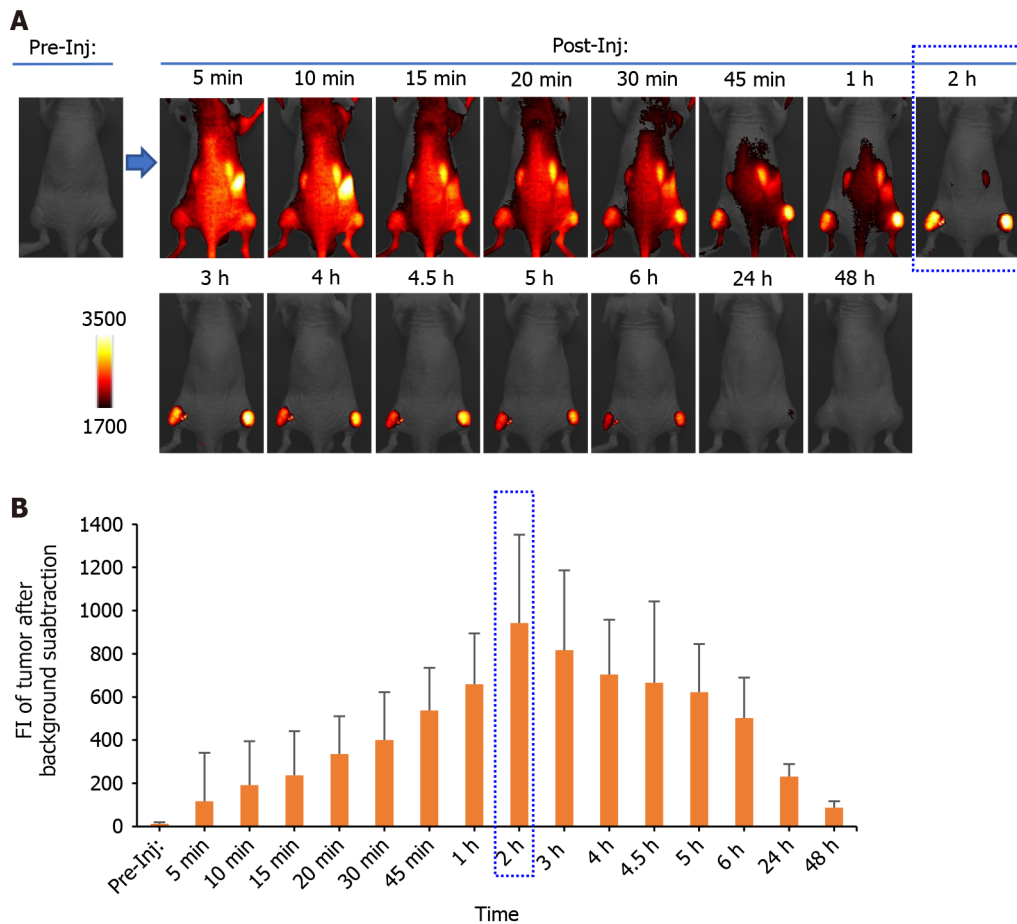


Figure 4 *In vivo* longitudinal near-infrared fluorescence imaging of folate-Si-rhodamine-1 in a KB tumor-bearing representative mouse. A: Imaging was conducted before and after folate-Si-rhodamine-1 (FolateSiR-1) injection. The indicated time points after injection are at 5 min, 10 min, 15 min, 20 min, 30 min, 45 min, 1 h, 2 h, 3 h, 4 h, 4.5 h, 5 h, 6 h, 24 h, and 48 h. Time-dependent FolateSiR-1 distribution and its specific tumor accumulation is shown in serial images; B: Quantitative fluorescent signal intensity analysis of the tumors. Data are presented as the mean \pm SD ($n = 4$). NIR: Near-infrared; FI: Fluorescent signal intensity; Pre-Inj: Pre-injection; Post-Inj: Post-injection.

DISCUSSION

FolateSiR-1 significantly accumulated in the FR-expressing KB tumors, but not in the FR-negative tumors and normal organs. This PS was activated by NIR light to evoke cytotoxic effects on cells and tumors, resulting in PDT induced necrosis and apoptosis. Our findings suggest that FolateSiR-1 has potential for application in the PDT of FR-expressing tumors.

High FR expression was observed in the KB cells, but not in the OVCAR-3 and A4 cells (Figure 2A). Furthermore, fluorescence microscopy revealed that KB cells incubated with FolateSiR-1 showed strong FI which contrasted with that of the other two cell lines (Figure 2B). These results encouraged us to use KB cells as a representative FR-expressing xenograft tumor in a mouse model. Stronger FI was observed in KB tumors, compared to OVCAR-3 tumors, A4 tumors, and other sites throughout the body, which was attributed to the presence of FolateSiR-1 (Figures 2C-E). Furthermore, strongly positive FR staining was observed in KB tumor cells, whereas it was almost entirely absent in OVCAR-3 cells based on IHC (Figure 2F). These findings and *ex vivo* images of normal tissues (Figure 5C) indicate that FolateSiR-1 binds FR with high specificity in FR-overexpressing cells and tumors.

In this study, FolateSiR-1 accumulation peaked at 2 h after injection in KB tumors, followed by its disappearance over the next 24 h based on quantification of serial fluorescence images. The rapid peak accumulation of FolateSiR-1 in tumors may be a more convenient clinical setting of PDT than the number of days required for PIT using an antibody as a PS carrier. Furthermore, rapid tumor contrast enhancement within a few hours after PS injection could be advantageous for real-time cancer detection in the intraoperative setting. Moreover, irradiation delivered at a shorter interval when PS is still present in the blood vessels results in a superior tumor response which causes marked vascular damage[39]. *In vivo* time-dependent images (Figure 4) and *ex vivo* images of tissues (Figure 5C) showed that FolateSiR-1 was cleared relatively quickly from normal tissues, including the main excretory organs (liver and kidney), indicating that the phototoxic side effects were minimized.

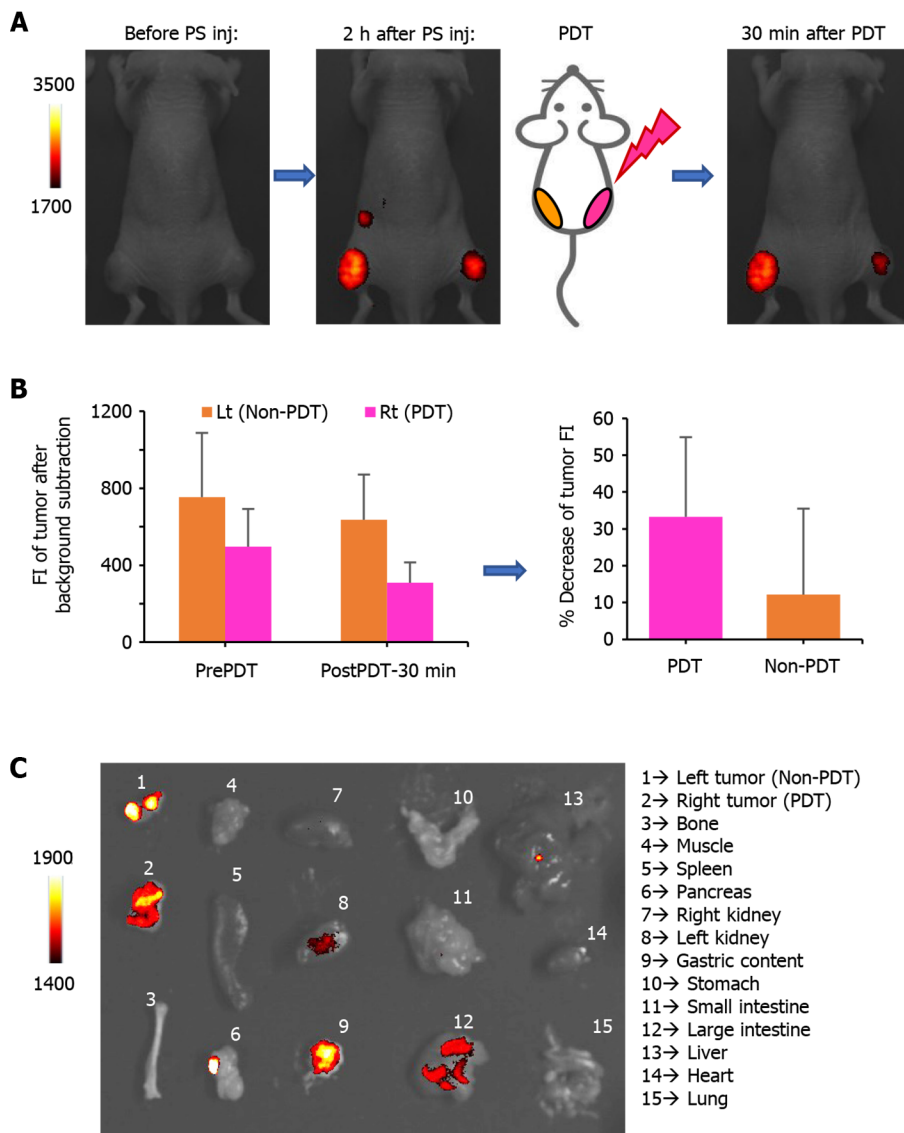


Figure 5 *In vivo* and *ex vivo* images before and after photodynamic therapy. A: Near-infrared fluorescence images of representative tumor bearing mice: before photosensitizer (PS) (FolateSiR-1) injection (left), 2 h after PS injection (center), and 30 min after photodynamic therapy (PDT) (right). The right tumor received PDT while the left tumor did not. Fluorescent signal intensity (FI) of the right tumor decreased immediately after PDT, and the extent of FI reduction is larger than that of the left tumor; B: Bar graph showing the FI of the tumor before- and 30 min after PDT. Data are presented as the mean \pm SD ($n = 4$); C: *Ex vivo* fluorescence images captured 30 min after PDT. NIR: Near-infrared; Lt: Left; Rt: Right; PS inj: photosensitizer injection; PDT: Photodynamic therapy; Non-PDT: Without PDT; FI: Fluorescent signal intensity.

KB cells showed extensive bright fluorescence signals, whereas there was no obvious PS binding or uptake in the negative control cells indicating that FolateSiR-1 was selectively localized in KB cells (Figure 2B). Fluorescent signals were mainly observed at the plasma membrane of KB cells and in some cytoplasmic component sites. The cellular response to photodamage primarily depends on PS localization and PDT dose[40-42]. Photosensitizer localization and activation inside tumor tissues generates ROS which can directly kill malignant tumor cells[4]. Mitochondria-localized PS induces apoptotic cell death within a certain threshold of oxidative stress[6,43]. Necrosis is more often observed if the cell membrane is the site of action for the PS[44]. Mild oxidative damage by PS localized in the plasma membrane causes apoptosis, but severe damage leads to the loss of plasma membrane integrity and causes necrotic cell death[6,41,45]. Meanwhile, PSs targeting the endoplasmic reticulum, Golgi membranes, and lysosomes mediates necrosis[43]. Moreover, high PDT doses (dependent on the amount of PS and the irradiation dose) inactivate essential enzymes and other components of the apoptotic cascade resulting in increased cellular damage leading to necrosis rather than apoptosis[40, 46]. The merged fluorescence- and phase-contrast images showed strong FolateSiR-1 fluorescence intensity in the KB cell membrane and the cytoplasm, but not in the nucleus (Figure 2B). This finding suggests that FolateSiR-1 promotes necrosis and is a suitable probe for PDT. The probe alone did not penetrate the nuclear membrane and therefore did not cause genetic damage.

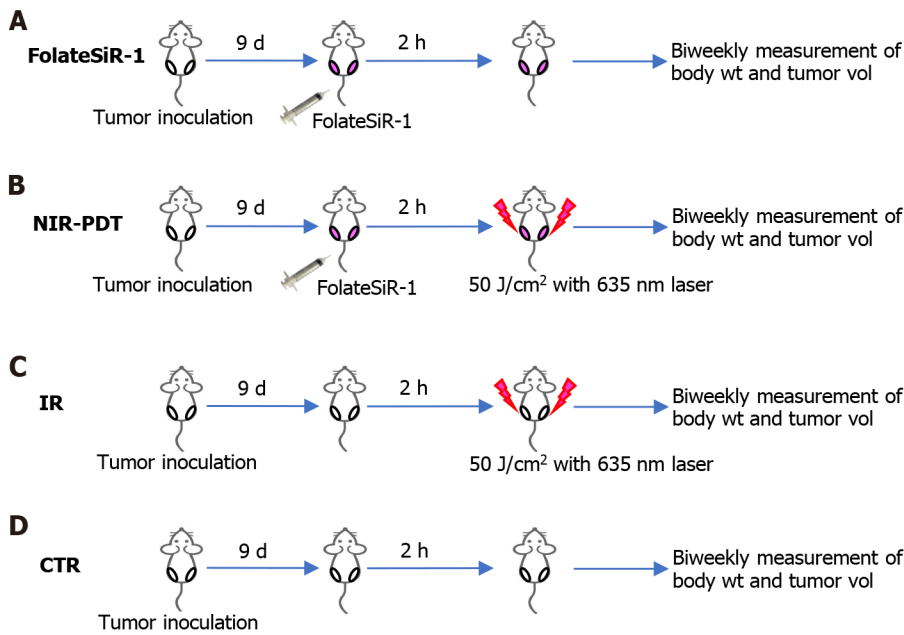


Figure 6 Experimental treatment scheme. Tumor bearing mice were assigned to four groups: A: folate-Si-rhodamine-1 injection alone; B: Near-infrared (NIR) photodynamic therapy (50 J/cm²); C: NIR irradiation alone (50 J/cm²); and D: no treatment. FolateSiR-1: Folate-Si-rhodamine-1; NIR-PDT: Near-infrared photodynamic therapy; IR: Laser irradiation; CTR: Control; wt: Weight; vol: Volume.

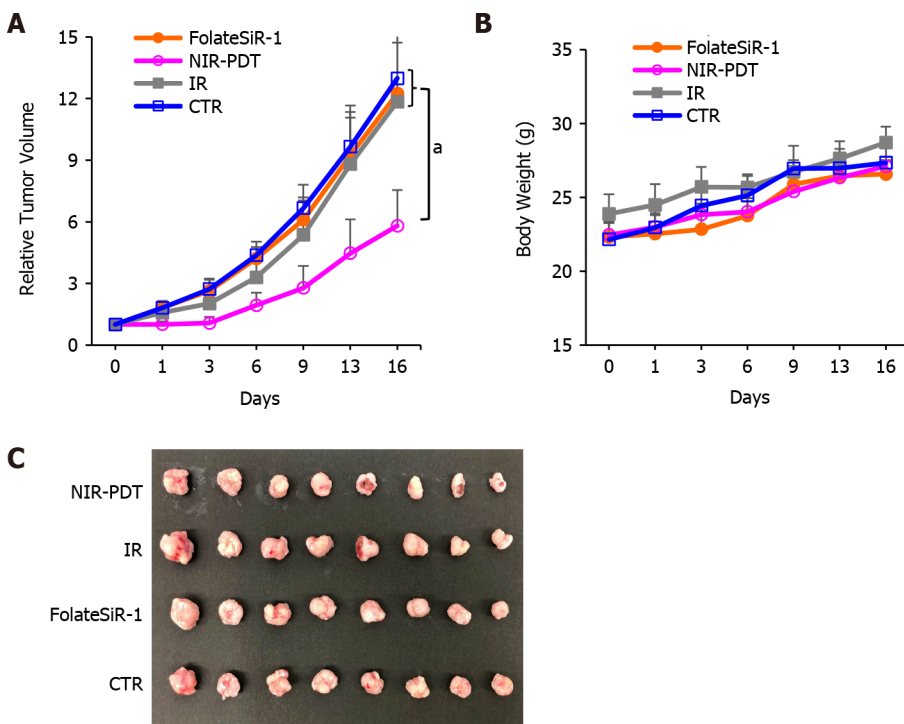


Figure 7 Phototherapeutic effects of photodynamic therapy on KB xenografts and body weight in mice. A: Tumor volume change is expressed as the relative tumor volume (volume on the indicated day/starting volume prior to the treatment). Tumors-treated by near-infrared photodynamic therapy (NIR-PDT) (50 J/cm²), irradiation alone (50 J/cm²), folate-Si-rhodamine-1 alone, and no treatment are shown in pink (○), gray (■), orange (●), and blue (□), respectively. Tumors-treated by NIR-PDT show significantly delayed growth compared to those of other groups. Values represent the mean ± SD (*n* = 8), ^a*P* < 0.05 NIR-PDT vs other groups; B: Average body weight did not differ significantly among the four groups of mice; C: Images of *ex vivo* tumors excised 16 d after treatment. FolateSiR-1: Folate-Si-rhodamine-1; NIR-PDT: Near-infrared photodynamic therapy; IR: Laser irradiation; CTR: Control.

Our NIR-PDT regimen delivered a single dose of NIR light (50 J/cm²) to KB tumors after intravenous administration of FolateSiR-1 (100 μg). The growth rate of tumors receiving PDT was significantly suppressed even with this single irradiation compared with the control groups (Figure 7). Complete tumor remission was not achieved with a single irradiation, however, partial remission for three days and delayed relapse was noted after PDT. Therefore, NIR-PDT using FolateSiR-1 is expected to be as

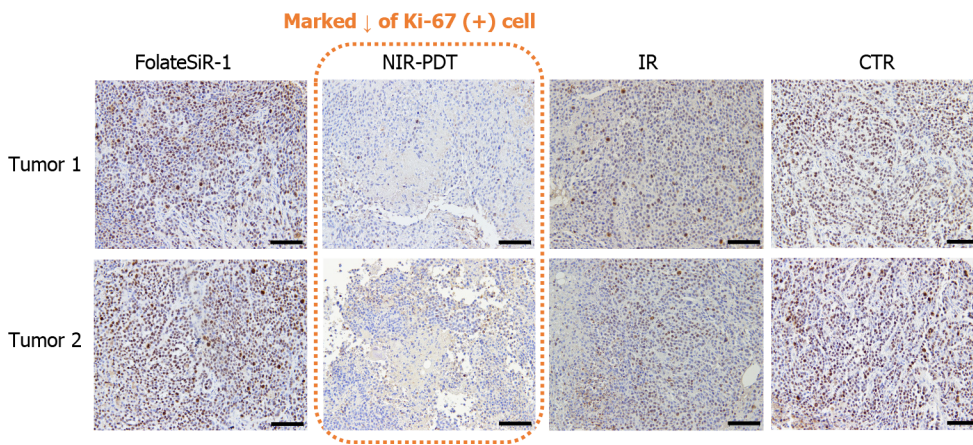


Figure 8 Tumor immunohistochemical staining of Ki-67 at 24 h after near-infrared photodynamic therapy. The weak staining and marked reduction of Ki-67-positive cells were detected in tumors treated with near-infrared photodynamic therapy (scale bar = 100 μ m, 20 \times magnification). FolateSiR-1: Folate-Si-rhodamine-1; NIR-PDT: Near-infrared photodynamic therapy; IR: Laser irradiation; CTR: Control.

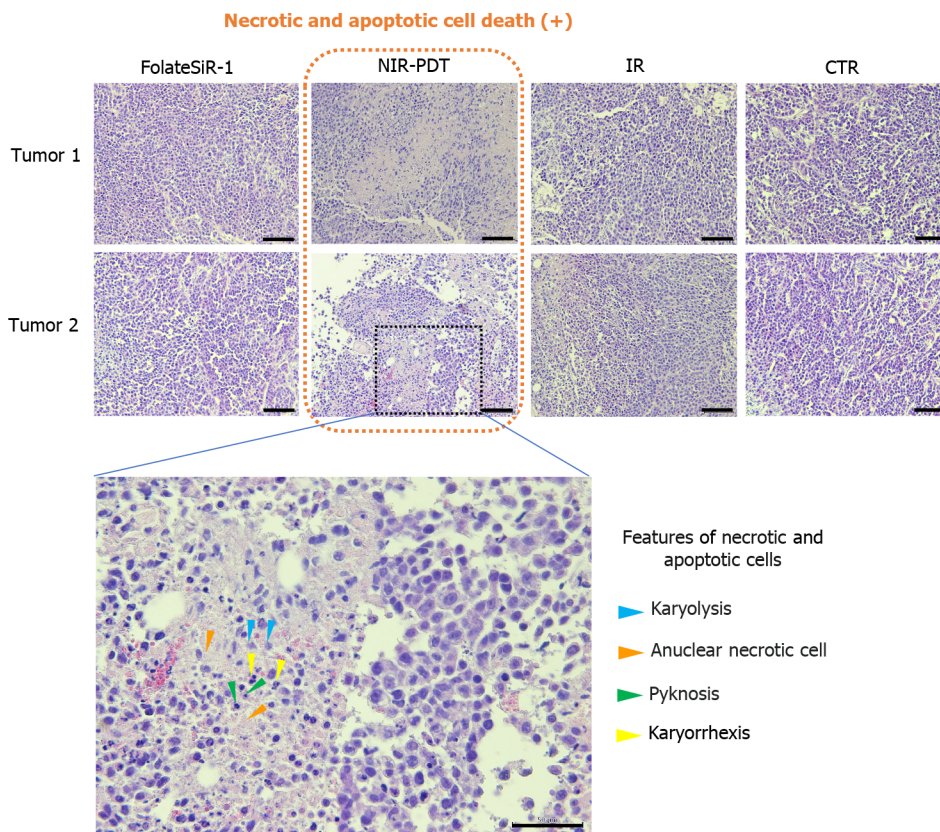


Figure 9 Histological examination of the destructive effects of near-infrared photodynamic therapy in tumor tissues 24 h after near-infrared photodynamic therapy. Tumors are stained with hematoxylin and eosin. The left lowermost image is a magnification of the indicated portion of the upper image. Some features of necrotic and apoptotic cells are shown with arrowheads: nuclear fading due to DNA loss, karyolysis (blue), anuclear necrotic cells with a glossier homogenous appearance (orange), nuclear chromatin condensation, pyknosis (green), nuclear fragmentation, and karyorrhexis (yellow). (Scale bar = 100 μ m, 20 \times magnification for upper two rows, and scale bar = 50 μ m, 40 \times magnification for lower row). FolateSiR-1: folate-Si-rhodamine-1; NIR-PDT: Near-infrared photodynamic therapy; IR: laser irradiation; CTR: control.

effective as other currently tested PDTs and PITs, because more precise treatment regimens can be easily designed by adjusting PS and irradiation doses, and repeating the treatment to improve the therapeutic efficacy and potentially achieving complete pathological remission. An extended study aiming to optimize the treatment will be performed in the future.

Photobleaching is the light-mediated destruction of PS. Linear correlation between protoporphyrin IX photobleaching and necrosis was used as a predictive tool of the PDT response in the rat ovarian cancer model[47]. Our limited mice experiments showed a tendency for FI reduction in tumors immediately

after PDT (Figure 5A and B), and this was probably due to some PS photobleaching and necrosis of cancer cells. An extended study is required to confirm this association.

Rapid phototoxic cell death-induced by NIR-PDT (10 J/cm²) and abundant dead cells stained green with NucGreen® Dead reagent were clearly observed in viability imaging assays (Figure 3). In contrast, neither FolateSiR-1 alone nor irradiation alone induced noticeable cell death, suggesting that FolateSiR-1 is an effective PS with high phototoxicity and low dark toxicity.

Nuclear staining of the proliferative factor Ki67 in tumor cells using IHC indicating that these cells were actively proliferating at 24 h post-PDT. Meanwhile, tumors treated with PDT (50 J/cm²) showed weak staining and a marked decrease in Ki-67 positive cells, suggesting that FolateSiR-1 mediated PDT inhibited cell proliferation in tumors (Figure 8). Therefore, some cells stop proliferating, but do not immediately undergo necrosis or apoptosis. In addition, tumors irradiated with targeted PDT exhibited rapid and extensive damage with a phenotype of necrosis and apoptotic cell death at the irradiated site as indicated by H&E staining. Some cells displayed necrotic cell death features such as nuclear fading (karyolysis) and anuclear necrotic cells, while other cells showed apoptotic cell death features such as chromatin condensation of the nucleus (pyknosis) and nuclear fragmentation (karyorrhexis). No distinct damage was found in the tumors of the other control groups (Figure 9). These results were consistent with that of tumor growth and revealed the presumptive mechanism of the effects of PDT.

The main mechanism of tumor destruction by PDT is the direct damage to cells[45], however, there are other indirect mechanisms such as damage to tumor blood vessels and nonspecific activation of the immune response against tumor cells[42,48]. As these mechanisms were not addressed in this study, additional research on this topic is required. Furthermore, only one FR-overexpressing cell line-derived subcutaneous tumor was used. The nature of the xenografted-tumor microenvironment does not reflect all of the characteristics of human cancer tissue. Not all tumors express high FR levels in a clinical setting. These drawbacks may limit the wide use of FR-targeted NIR-PDT. Nevertheless, further research may elucidate these limitations. The fascinating features of FolateSiR-1, including selectivity for tumor cells, membranous and subcellular localization, and cytotoxicity in combination with NIR irradiation, prompted the development of an alternative PS for NIR-PDT. The results of this study indicate that FR-targeted NIR-PDT using this PS may have potential for application in the treatment of FR-overexpressing tumors. Moreover, specific binding of FolateSiR-1 to FRs and emission of near-infrared light may be useful for decision making in various settings including patient screening for treatment selection, theranostic applications such as image-guided cancer detection and PDT, or in combination with other treatments.

CONCLUSION

FolateSiR-1 displayed FR-specificity *in vitro* and *in vivo* and functioned as a potential PS when irradiated with NIR light, causing cellular tumor damage by provoking the cumulative effect of necrosis, apoptosis, and cell proliferation-inhibition. These findings suggest that FolateSiR-1 may be effectively utilized in PDT with low side effects, and FR-targeted NIR-PDT can potentially provide new effective strategies for the treatment of FR-overexpressing tumors.

ARTICLE HIGHLIGHTS

Research background

Photodynamic therapy (PDT) is one of the emerging options to combat cancer and it requires photosensitizer (PS) and corresponding light irradiation. The tumor selectivity of the photosensitizer improves tumor localization in PDT, enhances tumor destruction, and reduces side effects due to off-target localization. Folate receptor (FR) membrane protein is frequently overexpressed in human cancer and specific active targeting of PS to FR can be achieved by conjugation with the folate moiety.

Research motivation

We previously developed a folate-linked, near-infrared (NIR)-sensitive probe folate-Si-rhodamine-1 (FolateSiR-1). The feasibility of NIR-PDT using FolateSiR-1 and appropriate light irradiation had not been determined and required elucidation.

Research objectives

The aim of this study was to evaluate the photodynamic therapeutic efficacy of FolateSiR-1 in a preclinical cancer model and determine the cell death mode induced by FolateSiR-1-based PDT.

Research methods

FolateSiR-1 was synthesized by conjugating a folate moiety to the Si-rhodamine derivative through a

negatively charged tripeptide linker. Utilizing FR-overexpressing cell line KB and low FR-expressing cell lines OVCAR-3 and A4, selective binding of FolateSiR-1 to FR was evaluated by fluorescence microscopy. Cell viability imaging assays was exploited to assess the phototoxic effect of FolateSiR-1. *In vivo* longitudinal fluorescence imaging was conducted to examine the time-dependent biodistribution of FolateSiR-1 and its specific accumulation in KB tumors. To evaluate PDT efficacy of FolateSiR-1, KB tumor-bearing mice were divided into four groups: (1) FolateSiR-1 alone; (2) FolateSiR-1 followed by NIR irradiation; (3) NIR irradiation alone; and (4) no treatment. Tumor volume measurement, as well as immunohistochemical (IHC) and histological examinations of tumors were performed to determine the effect of PDT.

Research results

FR-specific binding of FolateSiR-1 was observed by fluorescence microscopy and *in vivo* fluorescence imaging. Cell viability imaging assays indicated that NIR-PDT induced cell death. *In vivo* longitudinal fluorescence imaging showed rapid peak accumulation of FolateSiR-1 in KB tumors 2 h after injection. The tumor volumes in the PDT group were significantly reduced compared to the other groups ($P < 0.05$). IHC analysis revealed reduced numbers of proliferation marker Ki-67-positive cells in PDT treated tumors, and hematoxylin-eosin staining revealed features of necrotic- and apoptotic cell death.

Research conclusions

FolateSiR-1 may be effectively utilized in PDT with low side effects, and the FR-targeted NIR-PDT can potentially reveal new strategies for the treatment of FR-overexpressing tumors.

Research perspectives

The fascinating features of FolateSiR-1, including specificity to FR, cytotoxicity in combination with NIR irradiation and relatively fast clearance implying low toxicity, prompted the development of an alternative PS for NIR-PDT. The therapeutic effect was significant after a single dose of irradiation and may be optimized to achieve patient-specific clinical effects. Moreover, fluorescence emission from FolateSiR-1 may be used for real time cancer detection and patient screening for treatment selection. Further research may elucidate these additional details of these processes.

ACKNOWLEDGEMENTS

We thank Aya Sugyo for help with the animal experiments and Tsuneo Saga for providing the A4 cell.

FOOTNOTES

Author contributions: Aung W designed the study, conducted most of the experiments, analyzed the data, and wrote the manuscript; Hanaoka K, designed, synthesized, and provided the folate-Si-rhodamine-1; Tsuji AB and Higashi T coordinated the research and contributed to manuscript preparation; all authors critically reviewed and approved the final version of the article.

Supported by a Grant-in-Aid for Scientific Research (C) from the Japan Society for the Promotion of Science, No. 21K07740 (to Aung W).

Institutional animal care and use committee statement: This study was reviewed and approved by the Institutional Review Board of National Institute for Quantum and Radiological Science and Technology, No. 13-1022-9.

Conflict-of-interest statement: All the authors report no relevant conflicts of interest for this article.

Data sharing statement: All relevant data were presented in the manuscript. Further information is available from the corresponding author.

ARRIVE guidelines statement: The authors have read the ARRIVE guidelines, and the manuscript was prepared and revised according to the ARRIVE guidelines.

Open-Access: This article is an open-access article that was selected by an in-house editor and fully peer-reviewed by external reviewers. It is distributed in accordance with the Creative Commons Attribution NonCommercial (CC BY-NC 4.0) license, which permits others to distribute, remix, adapt, build upon this work non-commercially, and license their derivative works on different terms, provided the original work is properly cited and the use is non-commercial. See: <https://creativecommons.org/licenses/by-nc/4.0/>

Country/Territory of origin: Japan

ORCID number: Winn Aung 0000-0002-0896-7158; Atsushi B Tsuji 0000-0003-2726-288X; Kenjiro Hanaoka 0000-0003-0797-4038; Tatsuya Higashi 0000-0002-8338-4737.

S-Editor: Gong ZM

L-Editor: A

P-Editor: Wu RR

REFERENCES

- Sung H**, Ferlay J, Siegel RL, Laversanne M, Soerjomataram I, Jemal A, Bray F. Global Cancer Statistics 2020: GLOBOCAN Estimates of Incidence and Mortality Worldwide for 36 Cancers in 185 Countries. *CA Cancer J Clin* 2021; **71**: 209-249 [PMID: 33538338 DOI: 10.3322/caac.21660]
- Algorri JF**, Ochoa M, Roldán-Varona P, Rodríguez-Cobo L, López-Higuera JM. Photodynamic Therapy: A Compendium of Latest Reviews. *Cancers (Basel)* 2021; **13** [PMID: 34503255 DOI: 10.3390/cancers13174447]
- Agostinis P**, Berg K, Cengel KA, Foster TH, Girotti AW, Gollnick SO, Hahn SM, Hamblin MR, Juzeniene A, Kessel D, Korbelik M, Moan J, Mroz P, Nowis D, Piette J, Wilson BC, Golab J. Photodynamic therapy of cancer: an update. *CA Cancer J Clin* 2011; **61**: 250-281 [PMID: 21617154 DOI: 10.3322/caac.20114]
- van Straten D**, Mashayekhi V, de Bruijn HS, Oliveira S, Robinson DJ. Oncologic Photodynamic Therapy: Basic Principles, Current Clinical Status and Future Directions. *Cancers (Basel)* 2017; **9** [PMID: 28218708 DOI: 10.3390/cancers9020019]
- Mroz P**, Yaroslavsky A, Kharkwal GB, Hamblin MR. Cell death pathways in photodynamic therapy of cancer. *Cancers (Basel)* 2011; **3**: 2516-2539 [PMID: 23914299 DOI: 10.3390/cancers3022516]
- Agostinis P**, Buytaert E, Breyssens H, Hendrickx N. Regulatory pathways in photodynamic therapy induced apoptosis. *Photochem Photobiol Sci* 2004; **3**: 721-729 [PMID: 15295626 DOI: 10.1039/b315237e]
- Hamblin MR**, Abrahamse H. Factors Affecting Photodynamic Therapy and Anti-Tumor Immune Response. *Anticancer Agents Med Chem* 2021; **21**: 123-136 [PMID: 32188394 DOI: 10.2174/1871520620666200318101037]
- Abrahamse H**, Hamblin MR. New photosensitizers for photodynamic therapy. *Biochem J* 2016; **473**: 347-364 [PMID: 26862179 DOI: 10.1042/BJ20150942]
- Bugaj AM**. Targeted photodynamic therapy--a promising strategy of tumor treatment. *Photochem Photobiol Sci* 2011; **10**: 1097-1109 [PMID: 21547329 DOI: 10.1039/c0pp00147c]
- Shirasu N**, Nam SO, Kuroki M. Tumor-targeted photodynamic therapy. *Anticancer Res* 2013; **33**: 2823-2831 [PMID: 23780966]
- Sibani SA**, McCarron PA, Woolfson AD, Donnelly RF. Photosensitizer delivery for photodynamic therapy. Part 2: systemic carrier platforms. *Expert Opin Drug Deliv* 2008; **5**: 1241-1254 [PMID: 18976134 DOI: 10.1517/17425240802444673]
- Debele TA**, Peng S, Tsai HC. Drug Carrier for Photodynamic Cancer Therapy. *Int J Mol Sci* 2015; **16**: 22094-22136 [PMID: 26389879 DOI: 10.3390/ijms160922094]
- Kašćáková S**, Hofland LJ, De Bruijn HS, Ye Y, Achilefu S, van der Wansem K, van der Ploeg-van den Heuvel A, van Koetsveld PM, Brugts MP, van der Lelij AJ, Sterenborg HJ, Ten Hagen TL, Robinson DJ, van Hagen MP. Somatostatin analogues for receptor targeted photodynamic therapy. *PLoS One* 2014; **9**: e104448 [PMID: 25111655 DOI: 10.1371/journal.pone.0104448]
- St Denis TG**, Hamblin MR. Synthesis, bioanalysis and biodistribution of photosensitizer conjugates for photodynamic therapy. *Bioanalysis* 2013; **5**: 1099-1114 [PMID: 23641699 DOI: 10.4155/bio.13.37]
- Ormond AB**, Freeman HS. Dye Sensitizers for Photodynamic Therapy. *Materials (Basel)* 2013; **6**: 817-840 [PMID: 28809342 DOI: 10.3390/ma6030817]
- Shen J**, Hu Y, Putt KS, Singhal S, Han H, Visscher DW, Murphy LM, Low PS. Assessment of folate receptor alpha and beta expression in selection of lung and pancreatic cancer patients for receptor targeted therapies. *Oncotarget* 2018; **9**: 4485-4495 [PMID: 29435118 DOI: 10.18632/oncotarget.23321]
- Vlahov IR**, Leamon CP. Engineering folate-drug conjugates to target cancer: from chemistry to clinic. *Bioconjug Chem* 2012; **23**: 1357-1369 [PMID: 22667324 DOI: 10.1021/bc2005522]
- Li PX**, Mu JH, Xiao HL, Li DH. Antitumor effect of photodynamic therapy with a novel targeted photosensitizer on cervical carcinoma. *Oncol Rep* 2015; **33**: 125-132 [PMID: 25376180 DOI: 10.3892/or.2014.3593]
- Stallivieri A**, Colombeau L, Jetpisbayeva G, Moussaron A, Myrzakhmetov B, Arnoux P, Acherar S, Vanderesse R, Frochot C. Folic acid conjugates with photosensitizers for cancer targeting in photodynamic therapy: Synthesis and photophysical properties. *Bioorg Med Chem* 2017; **25**: 1-10 [PMID: 27769669 DOI: 10.1016/j.bmc.2016.10.004]
- Gravier J**, Schneider R, Frochot C, Bastogne T, Schmitt F, Didelon J, Guillemin F, Barberi-Heyob M. Improvement of meta-tetra(hydroxyphenyl)chlorin-like photosensitizer selectivity with folate-based targeted delivery. synthesis and in vivo delivery studies. *J Med Chem* 2008; **51**: 3867-3877 [PMID: 18553957 DOI: 10.1021/jm800125a]
- Wang J**, Liu Q, Zhang Y, Shi H, Liu H, Guo W, Ma Y, Huang W, Hong Z. Folic Acid-Conjugated Pyropheophorbide as a the Photosensitizer Tested for In Vivo Targeted Photodynamic Therapy. *J Pharm Sci* 2017; **106**: 1482-1489 [PMID: 28263847 DOI: 10.1016/j.xphs.2017.02.019]
- Kim H**, Kim MW, Jeong YI, Yang HS. Redox-Sensitive and Folate-Receptor-Mediated Targeting of Cervical Cancer Cells for Photodynamic Therapy Using Nanophotosensitizers Composed of Chlorin e6-Conjugated β -Cyclodextrin via Diselenide Linkage. *Cells* 2021; **10** [PMID: 34571839 DOI: 10.3390/cells10092190]
- Syu WJ**, Yu HP, Hsu CY, Rajan YC, Hsu YH, Chang YC, Hsieh WY, Wang CH, Lai PS. Improved photodynamic cancer treatment by folate-conjugated polymeric micelles in a KB xenografted animal model. *Small* 2012; **8**: 2060-2069 [PMID: 22667324 DOI: 10.1021/bc2005522]

- 22508664 DOI: [10.1002/sml.201102695](https://doi.org/10.1002/sml.201102695)]
- 24 **Li H**, Jin Z, Cho S, Jeon MJ, Nguyen VD, Park JO, Park S. Folate-receptor-targeted NIR-sensitive polydopamine nanoparticles for chemo-photothermal cancer therapy. *Nanotechnology* 2017; **28**: 425101 [PMID: [28944765](https://pubmed.ncbi.nlm.nih.gov/28944765/) DOI: [10.1088/1361-6528/aa8477](https://doi.org/10.1088/1361-6528/aa8477)]
 - 25 **Kato T**, Jin CS, Ujiie H, Lee D, Fujino K, Wada H, Hu HP, Weersink RA, Chen J, Kaji M, Kaga K, Matsui Y, Wilson BC, Zheng G, Yasufuku K. Nanoparticle targeted folate receptor 1-enhanced photodynamic therapy for lung cancer. *Lung Cancer* 2017; **113**: 59-68 [PMID: [29110850](https://pubmed.ncbi.nlm.nih.gov/29110850/) DOI: [10.1016/j.lungcan.2017.09.002](https://doi.org/10.1016/j.lungcan.2017.09.002)]
 - 26 **Kato T**, Jin CS, Lee D, Ujiie H, Fujino K, Hu HP, Wada H, Wu L, Chen J, Weersink RA, Kanno H, Hatanaka Y, Hatanaka KC, Kaga K, Matsui Y, Matsuno Y, De Perrot M, Wilson BC, Zheng G, Yasufuku K. Preclinical investigation of folate receptor-targeted nanoparticles for photodynamic therapy of malignant pleural mesothelioma. *Int J Oncol* 2018; **53**: 2034-2046 [PMID: [30226590](https://pubmed.ncbi.nlm.nih.gov/30226590/) DOI: [10.3892/ijo.2018.4555](https://doi.org/10.3892/ijo.2018.4555)]
 - 27 **Baydoun M**, Moralès O, Frochot C, Ludovic C, Leroux B, Thecua E, Ziane L, Grabarz A, Kumar A, de Schutter C, Collinet P, Azais H, Mordon S, Delhem N. Photodynamic Therapy Using a New Folate Receptor-Targeted Photosensitizer on Peritoneal Ovarian Cancer Cells Induces the Release of Extracellular Vesicles with Immunoactivating Properties. *J Clin Med* 2020; **9** [PMID: [32326210](https://pubmed.ncbi.nlm.nih.gov/32326210/) DOI: [10.3390/jcm9041185](https://doi.org/10.3390/jcm9041185)]
 - 28 **Quilbe A**, Moralès O, Baydoun M, Kumar A, Mustapha R, Murakami T, Leroux B, de Schutter C, Thecua E, Ziane L, Colombeau L, Frochot C, Mordon S, Delhem N. An Efficient Photodynamic Therapy Treatment for Human Pancreatic Adenocarcinoma. *J Clin Med* 2020; **9** [PMID: [31936786](https://pubmed.ncbi.nlm.nih.gov/31936786/) DOI: [10.3390/jcm9010192](https://doi.org/10.3390/jcm9010192)]
 - 29 **Mussini A**, Uriati E, Bianchini P, Diaspro A, Cavanna L, Abbruzzetti S, Viappiani C. Targeted photoimmunotherapy for cancer. *Biomol Concepts* 2022; **13**: 126-147 [PMID: [35304984](https://pubmed.ncbi.nlm.nih.gov/35304984/) DOI: [10.1515/bmc-2022-0010](https://doi.org/10.1515/bmc-2022-0010)]
 - 30 **Aung W**, Tsuji AB, Sugyo A, Takashima H, Yasunaga M, Matsumura Y, Higashi T. Near-infrared photoimmunotherapy of pancreatic cancer using an indocyanine green-labeled anti-tissue factor antibody. *World J Gastroenterol* 2018; **24**: 5491-5504 [PMID: [30622378](https://pubmed.ncbi.nlm.nih.gov/30622378/) DOI: [10.3748/wjg.v24.i48.5491](https://doi.org/10.3748/wjg.v24.i48.5491)]
 - 31 **Olivo M**, Bhuvanawari R, Lucky SS, Dendukuri N, Soo-Ping Thong P. Targeted Therapy of Cancer Using Photodynamic Therapy in Combination with Multi-faceted Anti-Tumor Modalities. *Pharmaceuticals (Basel)* 2010; **3**: 1507-1529 [PMID: [27713315](https://pubmed.ncbi.nlm.nih.gov/27713315/) DOI: [10.3390/ph3051507](https://doi.org/10.3390/ph3051507)]
 - 32 **Numasawa K**, Hanaoka K, Saito N, Yamaguchi Y, Ikeno T, Echizen H, Yasunaga M, Komatsu T, Ueno T, Miura M, Nagano T, Urano Y. A Fluorescent Probe for Rapid, High-Contrast Visualization of Folate-Receptor-Expressing Tumors In Vivo. *Angew Chem Int Ed Engl* 2020; **59**: 6015-6020 [PMID: [31984590](https://pubmed.ncbi.nlm.nih.gov/31984590/) DOI: [10.1002/anie.201914826](https://doi.org/10.1002/anie.201914826)]
 - 33 **Chen C**, Ke J, Zhou XE, Yi W, Brunzelle JS, Li J, Yong EL, Xu HE, Melcher K. Structural basis for molecular recognition of folic acid by folate receptors. *Nature* 2013; **500**: 486-489 [PMID: [23851396](https://pubmed.ncbi.nlm.nih.gov/23851396/) DOI: [10.1038/nature12327](https://doi.org/10.1038/nature12327)]
 - 34 **Silva EF**, Schaberle FA, Monteiro CJ, Dąbrowski JM, Arnaut LG. The challenging combination of intense fluorescence and high singlet oxygen quantum yield in photostable chlorins—a contribution to theranostics. *Photochem Photobiol Sci* 2013; **12**: 1187-1192 [PMID: [23584281](https://pubmed.ncbi.nlm.nih.gov/23584281/) DOI: [10.1039/c3pp25419d](https://doi.org/10.1039/c3pp25419d)]
 - 35 **Weissleder R**, Ntziachristos V. Shedding light onto live molecular targets. *Nat Med* 2003; **9**: 123-128 [PMID: [12514725](https://pubmed.ncbi.nlm.nih.gov/12514725/) DOI: [10.1038/nm0103-123](https://doi.org/10.1038/nm0103-123)]
 - 36 **Scholzen T**, Gerdes J. The Ki-67 protein: from the known and the unknown. *J Cell Physiol* 2000; **182**: 311-322 [PMID: [10653597](https://pubmed.ncbi.nlm.nih.gov/10653597/) DOI: [10.1002/\(SICI\)1097-4652\(200003\)182:3<311::AID-JCP1>3.0.CO;2-9](https://doi.org/10.1002/(SICI)1097-4652(200003)182:3<311::AID-JCP1>3.0.CO;2-9)]
 - 37 **Sudo H**, Tsuji AB, Sugyo A, Ogawa Y, Sagara M, Saga T. ZDHHC8 knockdown enhances radiosensitivity and suppresses tumor growth in a mesothelioma mouse model. *Cancer Sci* 2012; **103**: 203-209 [PMID: [22017350](https://pubmed.ncbi.nlm.nih.gov/22017350/) DOI: [10.1111/j.1349-7006.2011.02126.x](https://doi.org/10.1111/j.1349-7006.2011.02126.x)]
 - 38 **Low PS**, Kularatne SA. Folate-targeted therapeutic and imaging agents for cancer. *Curr Opin Chem Biol* 2009; **13**: 256-262 [PMID: [19419901](https://pubmed.ncbi.nlm.nih.gov/19419901/) DOI: [10.1016/j.cbpa.2009.03.022](https://doi.org/10.1016/j.cbpa.2009.03.022)]
 - 39 **Chen B**, Roskams T, de Witte PA. Antivascular tumor eradication by hypericin-mediated photodynamic therapy. *Photochem Photobiol* 2002; **76**: 509-513 [PMID: [12462645](https://pubmed.ncbi.nlm.nih.gov/12462645/) DOI: [10.1562/0031-8655\(2002\)076<0509:atebhm>2.0.co;2](https://doi.org/10.1562/0031-8655(2002)076<0509:atebhm>2.0.co;2)]
 - 40 **Lavie G**, Kaplinsky C, Toren A, Aizman I, Meruelo D, Mazur Y, Mandel M. A photodynamic pathway to apoptosis and necrosis induced by dimethyl tetrahydroxyhelianthron and hypericin in leukaemic cells: possible relevance to photodynamic therapy. *Br J Cancer* 1999; **79**: 423-432 [PMID: [10027308](https://pubmed.ncbi.nlm.nih.gov/10027308/) DOI: [10.1038/sj.bjc.6690066](https://doi.org/10.1038/sj.bjc.6690066)]
 - 41 **Buytaert E**, Dewaele M, Agostinis P. Molecular effectors of multiple cell death pathways initiated by photodynamic therapy. *Biochim Biophys Acta* 2007; **1776**: 86-107 [PMID: [17693025](https://pubmed.ncbi.nlm.nih.gov/17693025/) DOI: [10.1016/j.bbcan.2007.07.001](https://doi.org/10.1016/j.bbcan.2007.07.001)]
 - 42 **Piette J**, Volanti C, Vantieghem A, Matroule JY, Habraken Y, Agostinis P. Cell death and growth arrest in response to photodynamic therapy with membrane-bound photosensitizers. *Biochem Pharmacol* 2003; **66**: 1651-1659 [PMID: [14555246](https://pubmed.ncbi.nlm.nih.gov/14555246/) DOI: [10.1016/s0006-2952\(03\)00539-2](https://doi.org/10.1016/s0006-2952(03)00539-2)]
 - 43 **Benov L**. Photodynamic therapy: current status and future directions. *Med Princ Pract* 2015; **24** Suppl 1: 14-28 [PMID: [24820409](https://pubmed.ncbi.nlm.nih.gov/24820409/) DOI: [10.1159/000362416](https://doi.org/10.1159/000362416)]
 - 44 **Hsieh YJ**, Wu CC, Chang CJ, Yu JS. Subcellular localization of Photofrin determines the death phenotype of human epidermoid carcinoma A431 cells triggered by photodynamic therapy: when plasma membranes are the main targets. *J Cell Physiol* 2003; **194**: 363-375 [PMID: [12548556](https://pubmed.ncbi.nlm.nih.gov/12548556/) DOI: [10.1002/jcp.10273](https://doi.org/10.1002/jcp.10273)]
 - 45 **Oleinick NL**, Morris RL, Belichenko I. The role of apoptosis in response to photodynamic therapy: what, where, why, and how. *Photochem Photobiol Sci* 2002; **1**: 1-21 [PMID: [12659143](https://pubmed.ncbi.nlm.nih.gov/12659143/) DOI: [10.1039/b108586g](https://doi.org/10.1039/b108586g)]
 - 46 **Castano AP**, Demidova TN, Hamblin MR. Mechanisms in photodynamic therapy: part two-cellular signaling, cell metabolism and modes of cell death. *Photodiagnosis Photodyn Ther* 2005; **2**: 1-23 [PMID: [25048553](https://pubmed.ncbi.nlm.nih.gov/25048553/) DOI: [10.1016/S1572-1000\(05\)00030-X](https://doi.org/10.1016/S1572-1000(05)00030-X)]
 - 47 **Ascencio M**, Collinet P, Farine MO, Mordon S. Protoporphyrin IX fluorescence photobleaching is a useful tool to predict the response of rat ovarian cancer following hexaminolevulinate photodynamic therapy. *Lasers Surg Med* 2008; **40**: 332-341 [PMID: [18563777](https://pubmed.ncbi.nlm.nih.gov/18563777/) DOI: [10.1002/lsm.20629](https://doi.org/10.1002/lsm.20629)]
 - 48 **Juarranz A**, Jaén P, Sanz-Rodríguez F, Cuevas J, González S. Photodynamic therapy of cancer. Basic principles and applications. *Clin Transl Oncol* 2008; **10**: 148-154 [PMID: [18321817](https://pubmed.ncbi.nlm.nih.gov/18321817/) DOI: [10.1007/s12094-008-0172-2](https://doi.org/10.1007/s12094-008-0172-2)]



Published by **Baishideng Publishing Group Inc**
7041 Koll Center Parkway, Suite 160, Pleasanton, CA 94566, USA
Telephone: +1-925-3991568
E-mail: bpgoffice@wjgnet.com
Help Desk: <https://www.f6publishing.com/helpdesk>
<https://www.wjgnet.com>

